

# Patterned Biomimetic Membranes: Effect of Concentration and pH

Anastasia Mardilovich and Efrosini Kokkoli\*

Department of Chemical Engineering and Materials Science, University of Minnesota, Minneapolis, Minnesota 55455

Received December 22, 2004. In Final Form: May 19, 2005

Planar-supported lipid bilayers have attracted enormous attention because of their properties as model cell membranes, which can be employed in a variety of fundamental biological studies and medical devices. Furthermore, the development of patterned biological interfaces is of great practical and scientific interest because of their potential applications in the field of biosensors, drug screening, tissue engineering, and medical implants. In this study, mica-supported membranes were constructed from biomimetic peptide-amphiphiles and their mixtures with lipidated poly(ethylene glycol) (PEG120) molecules or 1,2-dipalmitoyl-*sn*-glycero-3-phosphocholine (DPPC) phospholipids using the Langmuir–Blodgett technique. The two peptide-amphiphiles used in this study were a fibronectin-mimetic with the PHSRN(SG)<sub>3</sub>SGRGDSP headgroup (referred to as PHSRN-GRGDSP) that contains both the primary (GRGDSP) and the synergy (PHSRN) recognition sites for  $\alpha_5\beta_1$  integrins and a peptide-amphiphile that mimics a fragment of the N-terminus of the fractalkine receptor (referred to as NTFR). Compression isotherms of the peptide-amphiphiles and their mixtures with PEG120 at the air/water interface were recorded and analyzed to evaluate the extent of miscibility in the two-component LB films. Domain formation in mica-supported bilayers constructed from mixtures of peptide-amphiphiles and lipidated PEG120 or DPPC was observed using atomic force microscopy. In PHSRN-GRGDSP/PEG120 mixtures deposited from an aqueous subphase at pH 7, concentration-dependent phase separation was observed on the AFM images. The NTFR/PEG120 and NTFR/DPPC mixtures deposited at pH 10 exhibited extensive lateral phase separation at all mixture compositions, whereas at deposition pH 7 the concentrations of NTFR/DPPC examined here were well mixed.

## Introduction

The ability to engineer bioactive surfaces and to control their interactions with cells is essential for a variety of fundamental biological studies and medical applications.<sup>1</sup> Furthermore, the development of patterned biomaterials with regions of different functionalities provides an opportunity to create truly bioactive systems for a large variety of applications, including biosensors,<sup>2,3</sup> “lab-on-a-chip” bioanalytical systems,<sup>4</sup> drug screening devices,<sup>5,6</sup> tissue engineering,<sup>7</sup> and medical implants.<sup>8</sup>

Various methods can be applied to pattern and modify surface functionality and topography to promote controlled attachment of desired cell populations and to study different cell functions such as adhesion, morphology, proliferation, and migration. Photolithography<sup>9,10</sup> and soft lithography<sup>11–13</sup> are the most commonly utilized tech-

niques, which are extremely useful in creating high-resolution micrometer and submicrometer scale patterns. Other methods for fabricating functionalized templates for cell recognition include interference lithography,<sup>14</sup> dip-pen nanolithography,<sup>15</sup> polymer demixing,<sup>16</sup> and phase separation of block copolymers.<sup>17,18</sup> Recently, colloidal particles have been used to produce chemically patterned interfaces for biological applications.<sup>19–23</sup> Such an approach provides a convenient way to alter surface chemistry and topography over large areas by simply changing particle functionality, size, and packing density.

Self-assembled monolayers (SAMs) and Langmuir–Blodgett (LB) films have also been exploited intensively as surface coatings for nanofabrication techniques because of such useful properties as their small weight, ease of tailoring with functional groups, processability, and flexibility.<sup>24,25</sup> Moreover, supported LB bilayers con-

\* To whom correspondence should be addressed. Fax: (612) 626-7246; e-mail: kokkoli@cems.umn.edu.

(1) Tirrell, M.; Kokkoli, E.; Biesalski, M. *Surf. Sci.* **2002**, *500*, 61.  
 (2) Park, T. H.; Shuler, M. L. *Biotechnol. Prog.* **2003**, *19*, 243.  
 (3) Pancrazio, J. J.; Whelan, J. P.; Borkholder, D. A.; Ma, W.; Stenger, D. A. *Ann. Biomed. Eng.* **1999**, *27*, 697.  
 (4) Erickson, D.; Li, D. Q.; Krull, U. J. *Anal. Biochem.* **2003**, *317*, 186.  
 (5) Svedhem, S.; Dahlborg, D.; Ekeröth, J.; Kelly, J.; Hook, F.; Gold, J. *Langmuir* **2003**, *19*, 6730.  
 (6) Magnani, A.; Priamo, A.; Pasqui, D.; Barbucci, R. *Mater. Sci. Eng., C* **2003**, *23*, 315.  
 (7) Tan, W.; Desai, T. A. *Tissue Eng.* **2003**, *9*, 255.  
 (8) Yamato, M.; Konno, C.; Utsumi, M.; Kikuchi, A.; Okano, T. *Biomaterials* **2002**, *23*, 561.  
 (9) Scotchford, C. A.; Ball, M.; Winkelmann, M.; Voros, J.; Csucs, C.; Brunette, D. M.; Danuser, G.; Textor, M. *Biomaterials* **2003**, *24*, 1147.  
 (10) Clark, P. *Biosens. Bioelectron.* **1994**, *9*, 657.  
 (11) Whitesides, G. M.; Ostuni, E.; Takayama, S.; Jiang, X. Y.; Ingber, D. E. *Annu. Rev. Biomed. Eng.* **2001**, *3*, 335.  
 (12) Zhang, S. G.; Yan, L.; Altman, M.; Lassel, M.; Nugent, H.; Frankel, F.; Lauffenburger, D. A.; Whitesides, G. M.; Rich, A. *Biomaterials* **1999**, *20*, 1213.

(13) Mrksich, M.; Dike, L. E.; Tien, J.; Ingber, D. E.; Whitesides, G. M. *Exp. Cell Res.* **1997**, *235*, 305.

(14) Fan, Y. W.; Cui, F. Z.; Hou, S. P.; Xu, Q. Y.; Chen, L. N.; Lee, I.-S. *J. Neurosci. Methods* **2002**, *120*, 17.

(15) Piner, R. D.; Zhu, J.; Xu, F.; Hong, S. H.; Mirkin, C. A. *Science* **1999**, *283*, 661.

(16) Dalby, M. J.; Riehle, M. O.; Johnstone, H.; Affrossman, S.; Curtis, A. S. G. *Biomaterials* **2002**, *23*, 2945.

(17) Maheshwari, G.; Brown, G.; Lauffenburger, D. A.; Wells, A.; Griffith, L. G. *J. Cell Sci.* **2000**, *113*, 1677.

(18) Irvine, D. J.; Ruzette, A. V. G.; Mayes, A. M.; Griffith, L. G. *Biomacromolecules* **2001**, *2*, 545.

(19) Chen, C. S.; Mrksich, M.; Huang, S.; Whitesides, G. M.; Ingber, D. E. *Science* **1997**, *276*, 1425.

(20) Banerjee, P.; Irvine, D. J.; Mayes, A. M.; Griffith, L. G. *J. Biomed. Mater. Res.* **2000**, *50*, 331.

(21) Gleason, N. J.; Nodes, C. J.; Higham, E. M.; Guckert, N.; Aksay, I. A.; Shwarzbauer, J. E.; Carbeck, J. D. *Langmuir* **2003**, *19*, 513.

(22) Miyaki, M.; Fujimoto, K.; Kawaguchi, H. *Colloids Surf., A* **1999**, *153*, 603.

(23) Michel, R.; Reviakine, I.; Sutherland, D.; Fokas, C.; Csucs, G.; Danuser, G.; Spencer, N.; Textor, M. *Langmuir* **2002**, *18*, 8580.

structured from phospholipids serve as valuable biomembrane models that allow the study of specific biological phenomena occurring at the cell membrane that can be employed in the development of applications such as biosensors, information storage and delivery devices, and surface-modified implants.<sup>26–30</sup> In LB biomimetic membranes, there is control over composition and functionality that can be adjusted by incorporating specific proteins, peptide sequences, or carbohydrates into the lipid membrane structures. The nature and the packing of the lipid molecules, the composition of the subphase, and the temperature can be varied without limitation in the monolayer system. As a result, supported phospholipid LB membranes have been used widely to study, for example, the formation and structure of lipid microdomains of rafts<sup>31–34</sup> and peptide/lipid interactions,<sup>35–37</sup> to measure forces that govern cell adhesion processes,<sup>38,39</sup> and to create patterned surfaces.<sup>40</sup> In the last example, authors used the LB technique to create monolayers from a mixture of palmitic acid and thiolipids and to deposit them onto gold substrate. An appropriate solvent was then used to remove the physisorbed palmitic acid domains, leaving covalently bound thiolipid domains on the surface. This allowed other organic sulfur-bearing molecules present in the solvent (peptides with N-terminal cysteine and hydroxythiols) to chemisorb onto the newly exposed gold areas and to form self-assembled monolayers, thus creating patterned surfaces.<sup>40</sup>

Of particular relevance to the phospholipid membrane studies is the role of phase equilibria in lipid mixtures. Therefore, a better understanding of domain formation in mixed lipid monolayers and bilayers is essential for designing successful biomimetic supported membranes. Most of the information regarding phase behavior in lipid mixtures comes primarily from the phase diagrams constructed from calorimetric studies of the melting properties of aqueous lipid dispersions.<sup>41,42</sup> The degree of lipid miscibility can be extracted from these equilibrium phase diagrams, however, no information can be obtained on the morphology and dynamics of the lipid phase domains themselves. To visualize phase domains in mixed lipid monolayers, several surface analysis techniques have

been used recently, including epifluorescence microscopy, Brewster angle microscopy, or scanning probe microscopy.<sup>43–47</sup>

Up to now, much has been learned from previous studies on single phospholipid component monolayers or on binary phospholipid/cholesterol and phospholipid/phospholipid mixtures.<sup>32,44,48–54</sup> However, most of these studies involved monolayers created at low surface pressures, corresponding to gaseous/liquid-expanded (LE) or LE/liquid condensed (LC) phase coexistence regions on LB isotherms.<sup>55</sup> Thus, phase behavior of binary lipid mixtures at high surface pressures, corresponding to LC or solid regions on LB isotherms, needs further investigation. Moreover, mimicking cell membranes generally requires a higher monolayer surface pressure,<sup>56</sup> and up to date, very few studies have investigated binary lipid mixtures at surface pressures greater than LE–LC coexisting region.<sup>57</sup>

The focus of our work is to engineer biomimetic LB membranes from mixtures of peptide-amphiphiles with bioactive headgroups that mimic the cell adhesion domains of different proteins and DPPC (1,2-dipalmitoyl-*sn*-glycero-3-phosphocholine) or phospholipids decorated with short poly(ethylene glycol) (PEG120) molecules. Here, we study the effects of composition and pH on the formation of patterned monolayers using surface pressure–area isotherm measurements and atomic force microscopy (AFM) imaging.

Two different peptide-amphiphiles were used in this study: one containing a fibronectin-mimetic peptide sequence PHSRN(SG)<sub>3</sub>SGRGDSP (PHSRN-GRGDSP peptide-amphiphile)<sup>58</sup> and the other one with the QFPESVTENFEYDDLAEA peptide sequence that corresponds to residues 3–20 of the N-terminus of the fractalkine receptor (NTFR peptide-amphiphile).<sup>59</sup>

PHSRN-GRGDSP peptide-amphiphiles have been used to design a fibronectin-mimetic membrane to probe specific receptor ( $\alpha_5\beta_1$  integrin)–ligand (PHSRN-GRGDSP peptide-amphiphile) interactions at the molecular level.<sup>58</sup> The two peptide sequences used in this study are found in fibronectin: the 10th type III module, GRGDSP (the primary recognition site for  $\alpha_5\beta_1$  integrins), and the 9th type III module, PHSRN (the synergy binding site for  $\alpha_5\beta_1$ ). The distance between these two sequences in fibronectin (approximately 30–40 Å<sup>60</sup>) was mimicked by an (SG)<sub>3</sub>S spacer in the PHSRN-GRGDSP peptide-

(24) Jiang, X.; Hammond, P. T. *Langmuir* **2000**, *16*, 8501.

(25) Kumar, N.; Maldarelli, C.; Steiner, C.; Couzis, A. *Langmuir* **2001**, *17*, 7789.

(26) Chapman, D. *Langmuir* **1993**, *9*, 39.

(27) Ishihara, K.; Tsuji, T.; Kurosaki, T.; Nakabayashi, N. *J. Biomed. Mater. Res.* **1994**, *28*, 225.

(28) Weng, K. C.; Stålgren, J. J. R.; Duval, D. J.; Risbud, S. H.; Frank, C. W. *Langmuir* **2004**, *20*, 7232.

(29) Kasemo, B. *Surf. Sci.* **2002**, *500*, 656.

(30) Tien, H. T.; Ottova, A. L. *J. Membr. Sci.* **2001**, *189*, 83.

(31) Yuan, C.; Furlong, J.; Burgos, P.; Johnston, L. J. *Biophys. J.* **2002**, *82*, 2526.

(32) Vie, V.; Van Mau, N.; Lesniewska, E.; Goudonnet, J. P.; Heitz, F.; Le Grimmelc, C. *Langmuir* **1998**, *14*, 4574.

(33) Milhiet, P.-E.; Domec, C.; Giocondi, M.-C.; Van Mau, N.; Heitz, F.; Le Grimmelc, C. *Biophys. J.* **2001**, *81*, 547.

(34) Brown, D. A.; London, E. *J. Biol. Chem.* **2000**, *275*, 17221.

(35) Takamoto, D. Y.; Lipp, M. M.; von Nahmen, A.; Lee, K. Y. C.; Waring, A. J.; Zasadzinski, J. A. *Biophys. J.* **2001**, *81*, 153.

(36) Flanders, B. N.; Vickery, S. A.; Dunn, R. C. *J. Microsc.* **2001**, *202*, 379.

(37) van Mau, N.; Vie, V.; Chaloin, L.; Lesniewska, E.; Heitz, F.; Le Grimmelc, C. *J. Membr. Biol.* **1999**, *167*, 241.

(38) Sivasankar, S.; Briehar, W.; Lavrik, N.; Gumbiner, B.; Leckband, D. *Proc. Natl. Acad. Sci. U.S.A.* **1999**, *96*, 11820.

(39) Yu, Z. W.; Calvert, T. L.; Leckband, D. *Biochemistry* **1998**, *37*, 1540.

(40) Duschl, C.; Liley, M.; Corradin, G.; Vogel, H. *Biophys. J.* **1994**, *67*, 1229.

(41) Koynova, R.; Caffrey, M. *Chem. Phys. Lipids* **2002**, *115*, 107.

(42) Marsh, D. *Handbook of Lipid Bilayers*; CRC Press: Boca Raton, FL, 1990.

(43) Bagatolli, L. A.; Gratton, E. *Biophys. J.* **2000**, *79*, 434.

(44) Dietrich, C.; Bagatolli, L. A.; Volovyk, Z. N.; Thompson, N. L.; Levi, M.; Jacobson, K.; Gratton, E. *Biophys. J.* **2001**, *80*, 1417.

(45) Feigenson, G. W.; Buboltz, J. T. *Biophys. J.* **2001**, *80*, 2775.

(46) Korlach, J.; Schwill, P.; Webb, W. W.; Feigenson, G. W. *Proc. Natl. Acad. Sci. U.S.A.* **1999**, *96*.

(47) Samsonov, A. V.; Mihalyov, I.; Cohen, F. S. *Biophys. J.* **2001**, *81*, 1486.

(48) Solletti, J. M.; Botreau, M.; Sommer, F.; Duc, T. M.; Celio, M. R. *J. Vac. Sci. Technol., B* **1996**, *14*, 1492.

(49) Radhakrishnan, A.; Anderson, T. G.; McConnell, H. M. *Proc. Natl. Acad. Sci. U.S.A.* **2000**, *97*, 12422.

(50) Ross, M.; Steinem, C.; Galla, H.-J.; Janshoff, A. *Langmuir* **2001**, *17*, 2437.

(51) Schneider, J.; Dufrene, Y. F.; Barger, W. R.; Lee, G. U. *Biophys. J.* **2000**, *79*, 1107.

(52) DeWolf, C.; Leporatti, S.; Kirsch, C.; Klinger, R.; Brezesinski, G. *Chem. Phys. Lipids* **1999**, *97*, 129.

(53) Ekelund, K.; Sparr, E.; Engblom, J.; Wennerstrom, H.; Engstrom, S. *Langmuir* **1999**, *15*, 6946.

(54) Dufrene, Y. F.; Barger, W. R.; Green, J.-B. D.; Lee, G. U. *Langmuir* **1997**, *13*, 4779.

(55) McConlogue, C. W.; Vanderlick, T. K. *Langmuir* **1997**, *13*, 7158.

(56) Marsh, D. *Biochim. Biophys. Acta* **1996**, *1286*, 183.

(57) Sanchez, J.; Badia, A. *Thin Solid Films* **2003**, *440*, 223.

(58) Mardilovich, A.; Kokkoli, E.; *Biomacromolecules* **2004**, *5*, 950.

(59) Kokkoli, E.; Kasinskas, R. W.; Mardilovich, A.; Garg, A. *Biomacromolecules* **2005**, *6*, 1272.

(60) Leahy, D. J.; Aukhil, I.; Erickson H. P. *Cell* **1996**, *84*, 155.

amphiphile.<sup>58</sup> The theoretical length of the PHSRN-GRGDSP headgroup was calculated to be 7.3 nm<sup>58</sup> (18 amino acids  $\times$  0.37 nm/amino acid<sup>61</sup> plus 0.7 nm for the length of the (Glu) linker and (CH<sub>2</sub>)<sub>2</sub> spacer<sup>62</sup>). The results of our previous work on PHSRN-GRGDSP- $\alpha_5\beta_1$  integrins interaction indicated that to attain an effect from the PHSRN synergy site on the specific receptor–ligand adhesion, the entire sequence had to be exposed at the interface.<sup>58</sup> This was achieved by mixing peptide-amphiphiles with PEG120 at various concentrations. The length of the PEG120 headgroup was approximately 1.6 nm,<sup>62</sup> which is much smaller than the 7.3 nm theoretical length of the PHSRN-GRGDSP headgroup, and thus provided extra space for the peptide headgroup to be exposed at the interface. In the current study, to investigate the mixing behavior of different concentrations of peptide-amphiphiles and lipidated PEG120 at the air/water interface, thermodynamic analysis of the surface pressure–area isotherms was performed. AFM was then used to image the morphology and formation of patterns in peptide-amphiphile/PEG120 mixtures deposited onto hydrophobized mica disks using the LB technique. The effect of monolayer composition on the miscibility of the two molecules was investigated for these mixtures.

Another peptide-amphiphile used in this study, NTFR, contains a peptide sequence that corresponds to residues 3–20 of the N-terminus of the fractalkine receptor and was designed to recognize and specifically bind to fractalkine. The theoretical length of the NTFR headgroup was calculated to be approximately 7.3 nm<sup>59</sup> (18 amino acids  $\times$  0.37 nm/amino acid,<sup>61</sup> plus 0.7 nm for the length of the (Glu) linker and (CH<sub>2</sub>)<sub>2</sub> spacer<sup>62</sup>). Fractalkine is a recently discovered chemokine<sup>63</sup> that is present at sites of inflammation. Because of its unique molecular structure, fractalkine exhibits all the chemokine activities as well as acts as an adhesion molecule for leukocytes. As a result, fractalkine can be used as a target site and the NTFR peptide-amphiphile as the bullet for developing targeted delivery systems for anti-inflammatory agents.<sup>59</sup> Our previous results show that the receptor-mimicking NTFR peptide-amphiphile self-assembles with phospholipids and gives strong and specific interaction with fractalkine.<sup>59</sup> In this work, the effect of mixture composition and pH on the miscibility of the NTFR peptide-amphiphiles with lipidated PEG120 and DPPC phospholipid was investigated using the analysis of the LB isotherms and the AFM imaging.

The results presented here demonstrate that functionalizing surfaces with mixtures of two components, one of which is a peptide-amphiphile, may yield either well-mixed or patterned interfaces depending on the concentrations or the subphase pH used for the preparation of these films. Formation of patterned interfaces because of phase separation has been shown previously to take place in lipid mixtures. However, in this work, we extend such an approach to peptide-amphiphiles with different headgroup functionalities and their mixtures with phospholipids or lipidated PEG120. Thus, biomimetic patterned interfaces with areas of one functionality within a continuous matrix of a different functionality can be created via this approach using different peptide headgroups as well as various amphiphilic molecules.

## Materials and Methods

**Preparation of Bioartificial Membranes.** 1,2-Distearoyl-*sn*-glycero-3-phosphoethanolamine (DSPE), 1,2-dipalmitoyl-*sn*-glycero-3-phosphocholine (DPPC), and 1,2-distearoyl-*sn*-glycero-3-phosphoethanolamine-*N*-[amino(polyethyleneglycol)120] (PEG120) were purchased from Avanti Polar Lipids, Inc. (Alabaster, AL). (C<sub>16</sub>)<sub>2</sub>-Glu-C<sub>2</sub>-PHSRN(SG)<sub>3</sub>SGRGDSP and (C<sub>16</sub>)<sub>2</sub>-Glu-C<sub>2</sub>-QPES-VTFEYDDLAEA were synthesized according to a method described elsewhere.<sup>64</sup> These peptide-amphiphiles will be referred as PHSRN-GRGDSP and NTFR, respectively, in the remaining of the text.

Pure peptide-amphiphiles were dissolved at approximately 1 mg/mL in a 99:1 chloroform: methanol solution and were stored at 4 °C. The solution was heated to room temperature prior to use.

The Langmuir–Blodgett (LB) technique was used to record compression isotherms and to create supported bioactive bilayer membranes. Compression isotherms and film depositions were done on a KSV 5000 LB system (KSV Instruments, Helsinki, Finland) on DI water subphase at pH around 7 and at room temperature. A MilliQ Biocell system (Millipore, Bedford, MA) was used to produce DI pure water. The pH of the DI water from the MilliQ Biocell system was measured on the day of each experiment to be in the range of 6.5–7. Whenever necessary, the pH of the water subphase was adjusted to 10 by adding 30% NH<sub>4</sub>OH. After spreading the peptide-amphiphile solution on the air–water interface, chloroform was let to evaporate for 10 min. The depositions were done at 41 or 45 mN/m, which is well below the collapse pressure of the amphiphilic molecules. Upon reaching the deposition pressure, compressed monolayers were let to equilibrate for 10 min prior to deposition. Deposition speed for both the up and down strokes was 1 mm/min. Freshly cleaved mica disks of radius 7.5 mm were used as substrates for the supported bilayer membranes. DSPE layer was deposited first at the upstroke to make mica surfaces hydrophobic. The second layer with mixtures of peptide-amphiphiles and PEG120 or DPPC was deposited in the down stroke. Transfer ratios for both layers were calculated to be in the range 0.8–1, indicating that monolayers were deposited on mica surfaces with minimal disruption. The resulting supported bilayer membranes were transferred into glass vials under water and were kept in DI water, pH around 6.5–7 as collected from the MilliQ Biocell water purification system, prior to imaging. Care was taken to avoid exposing the surface to air, as the peptide-amphiphiles rearrange to form multilayers.<sup>65</sup>

**AFM Characterization of Supported Membranes.** AFM characterization of the LB films was done with a Digital Instruments Nanoscope III system equipped with a fluid cell for tapping mode (Digital Instruments, Santa Barbara, CA). All images were obtained in tapping mode in DI water, pH 6.5–7 as collected from the MilliQ Biocell water purification system, using standard 100- $\mu$ m V-shaped silicon nitride AFM cantilevers with pyramidal tips (Digital Instruments) of nominal radius 5–40 nm and nominal spring constant 0.58 N/m. Reproducible images were acquired within a maximum of 2 days from the day of deposition, on several different surfaces of the same composition and on different areas within the same surface. The amplitude setpoint during tapping was kept as high as possible to minimize the force exerted by the tip on the sample during imaging.<sup>66</sup>

## Results and Discussion

Surface pressure ( $\pi$ )–area compression isotherms for PEG120, PHSRN-GRGDSP, and their mixtures at the air/water interface and at room temperature and at pH 6.5–7 have been collected and the results are presented in Figure 1 (for clarity, not all concentrations recorded are shown). The shape of the isotherm for pure PEG120

(61) Idiris, A.; Alam, M. T.; Ikai, A. *Protein Eng.* **2000**, *13*, 763.

(62) Dori, Y.; Bianco-Peled, H.; Satija, S. K.; Fields, G. B.; McCarthy, J. B.; Tirrell, M. J. *Biomed. Mater. Res.* **2000**, *50*, 75.

(63) Bazan, J. F.; Bacon, K. B.; Hardiman, G.; Wang, W.; Soo, K.; Rossi, D.; Greaves, D. R.; Zlotnik, A.; Schall, T. J. *Nature* **1997**, *385*, 640.

(64) Berndt, P.; Fields, G. B.; Tirrell, M. *J. Am. Chem. Soc.* **1995**, *117*, 9515.

(65) Hansma, H. G.; Clegg, D. O.; Kokkoli, E.; Oroudjev, E.; Tirrell, M. *Methods Cell Biol.* **2002**, *69*, 163.

(66) Burnham, N. A.; Behrend, O. P.; Oulevey, F.; Gremaud, G.; Gallo, P.-J.; Gourdon, D.; Dupas, E.; Kulik, A. J.; Pollock, H. M.; Briggs, G. A. D. *Nanotechnology* **1997**, *8*, 67.

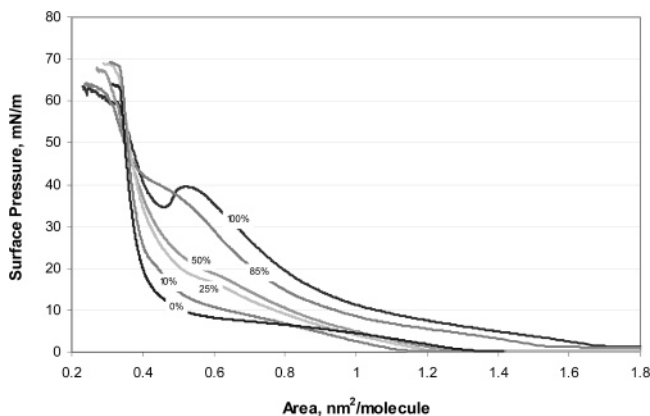


**Figure 1.** Surface pressure–area isotherms of mixtures of PHSRN-GRGDSP/PEG120 amphiphilic molecules on a DI water subphase at room temperature and pH 6.5–7 (as collected from MilliQ Biocell system). Molar percentages of PHSRN-GRGDSP in PHSRN-GRGDSP/PEG120 mixtures are shown for each isotherm.

resembles that which was previously published.<sup>67</sup> A “hump”, present on the isotherm of the pure PHSRN-GRGDSP peptide amphiphile, was observed previously for GRGDSP peptide-amphiphiles and was attributed to a secondary phase transition within the peptide-headgroup.<sup>68</sup> The plateau observed at  $\pi \approx 5\text{--}7$  mN/m in the PEG120 isotherm corresponds to a liquid expanded–liquid condensed (LE-LC) coexisting region.<sup>69</sup> Above 30 mN/m, the PEG120 monolayer is in a solid-condensed phase and collapses at approximately 64 mN/m with an area of 0.34 nm<sup>2</sup>/molecule, which corresponds to closely packed tails.<sup>70</sup> In contrast, the PHSRN-GRGDSP isotherm exhibits a more fluid behavior at all surface pressures below the film collapse pressure of approximately 60 mN/m with corresponding area per molecule of 0.33 nm<sup>2</sup>. The isotherms for binary mixtures of PEG120 and PHSRN-GRGDSP fall between those of the two pure monolayers, and the mean molecular areas measured for mixed monolayers increase with peptide-amphiphile concentration. The film collapse pressure for some mixtures remains relatively constant with respect to composition, which is an indication of possible phase separation.

Phase separation in mixed systems can, in general, be predicted from surface pressure–area isotherms of pure membrane components and may occur when amphiphilic molecules differ in tendency to crystallize.<sup>69</sup> In our study, PEG120 amphiphiles have a higher tendency to crystallize upon compression as observed from the surface pressure–area isotherm (Figure 1). In contrast, the PHSRN-GRGDSP peptide-amphiphiles remain in a more liquidlike phase. Therefore, when mixing PHSRN-GRGDSP with PEG120, the PHSRN-GRGDSP may get excluded from the growing crystalline domains of PEG120 and as a result form a continuous network around them.

To evaluate the extent of PHSRN-GRGDSP and PEG120 miscibility, the LB isotherms of their mixtures (Figure 1) were analyzed using the additivity rule and the surface phase rule. The area of the two-component monolayer at the deposition surface pressure of 41 mN/m was compared with that of the pure components at the same

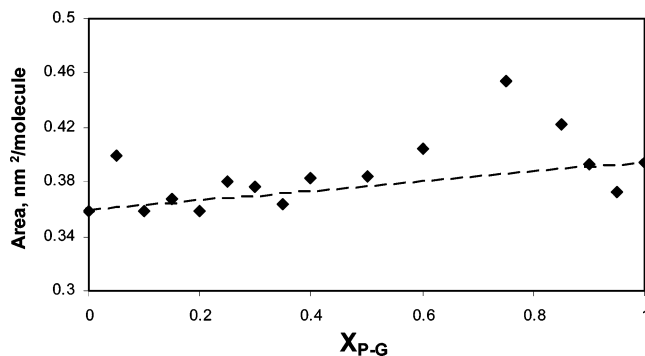


**Figure 2.** Mean molecular area of mixed PHSRN-GRGDSP/PEG120 monolayers as a function of PHSRN-GRGDSP mol fraction ( $X_{p-G}$ ) at a surface pressure of 41 mN/m. The straight line represents additivity rule values (ideal mixing).

surface pressure.<sup>71,72</sup>

$$\bar{A} = x_1 A_1 + x_2 A_2 \quad (1)$$

where  $\bar{A}$  is the mean molecular area of the two-component film,  $x_1$  and  $x_2$  are the molar fractions of components 1 (PHSRN-GRGDSP) and 2 (PEG120) in the mixed monolayers, and  $A_1$  and  $A_2$  are the mean molecular areas of the pure monolayers of components 1 and 2, respectively. The additivity rule predicts the molecular area in an ideal binary mixture, assuming no chemical or physical interactions between components. Both miscible components with ideal behavior and nonideal immiscible systems obey the above equation.<sup>73</sup> Interactions between components can lead to molecular areas that are different from those predicted by the additivity rule, and thus any deviation from ideality on the plot of  $\bar{A}$  versus molar fraction of one of the components indicates that the mixture is expected to be miscible and nonideal.<sup>71,72</sup> Figure 2 presents variations of the mean molecular areas of mixed PHSRN-GRGDSP/PEG120 monolayers as a function of the peptide-amphiphile molar fraction. A significant deviation from the additivity rule (dotted line in Figure 2) is observed for 5, 60, 75, 85, and 95 mol % of PHSRN-GRGDSP mixtures, suggesting that the two amphiphiles should be miscible and nonideal at these concentrations. However, for the other concentrations the additivity rule cannot differentiate between miscible ideal mixtures and nonideal immiscible ones, and therefore additional analysis of the isotherms is required to draw a more definite conclusion about miscibility in this system.

A more in depth analysis can be performed using the surface phase rule developed by Crisp.<sup>71,72</sup> When the temperature and the external pressure are kept constant, the number of degrees of freedom  $F$  of the monolayer is given by the equation

$$F = C^B + C^S - P^B - (q - 1) \quad (2)$$

where  $C^B$  is the number of components in the bulk,  $C^S$  is the number of components on the surface,  $P^B$  is the number of bulk phases, and  $q$  is the number of monolayer phases present in equilibrium with one another.<sup>71,72</sup> For a two-component LB film at the air–water interface,  $C^B = 2$  (air and water),  $C^S = 2$  (PHSRN-GRGDSP and PEG120), and  $P^B = 2$  (gas and liquid), and thus the above

(67) Dori, Y.; Bianco-Peled, H.; Satija, S. K.; Fields, G. B.; McCarthy, J. B.; Tirrell, M. J. *Biomed. Mater. Res.* **2000**, *50*, 75.

(68) Dillow, A. K.; Ochsenhirt, S. E.; McCarthy, J. B.; Fields, G. B.; Tirrell, M. *Biomaterials* **2001**, *22*, 1493.

(69) Mohwald, H. *Annu Rev. Phys. Chem.* **1990**, *41*, 441.

(70) Tanford, C. *The hydrophobic effect: formation of micelles and biological membranes*; Wiley: New York, 1980.

(71) Gaines, G. L. *Insoluble monolayers at the Liquid-Gas Interface*; Wiley-Interscience: New York, 1966.

(72) Petty, M. C. *Langmuir-Blodgett Films: An Introduction*; Cambridge University Press: Cambridge, 1996.

(73) Adamson, A. W.; Gast, A. P. *Physical chemistry of surfaces*, 6th ed.; Wiley: New York, 1997.

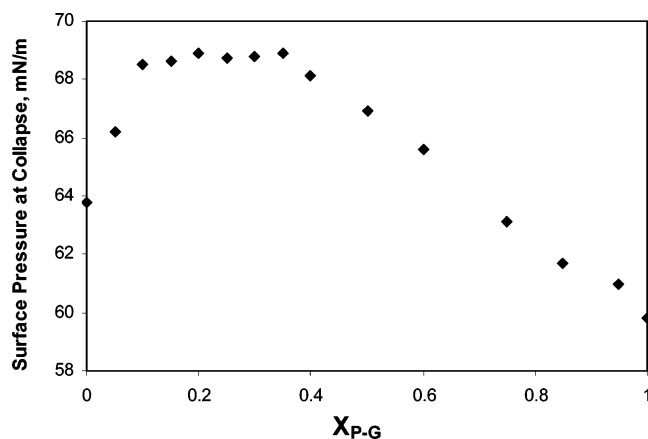


**Figure 3.** Collapse surface pressure as a function of the PHSRN-GRGDSP peptide-amphiphile molar fraction ( $X_{P-G}$ ) in PHSRN-GRGDSP/PEG120 mixtures.

equation reduces to

$$F = 3 - q \quad (3)$$

Here, the phase rule is applied to the film collapse pressure,<sup>72</sup> although it can also be applied to a phase transition pressure (LE–LC phase transition).<sup>74</sup> In general, if the two components are miscible, two homogeneous phases (either LE and LC or LC and collapsed state) will be present at equilibrium with each other and thus  $q = 2$  and the system has one degree of freedom. Therefore, either the collapse pressure or the transition pressure will vary with the monolayer composition. On the other hand, if the components are immiscible, three equilibrium surface phases ( $q = 3$ ) will coexist and there will be zero independent variables. Thus, the collapse (or transition) surface pressure will be independent of the monolayer composition.<sup>74</sup> Figure 3 illustrates the variations of the collapse surface pressure of the mixed monolayers as a function of the peptide-amphiphile molar fraction. A large variation occurs for  $0 < x_{P-G} < 0.1$  and  $0.35 < x_{P-G} < 1$  (Figure 3), which suggests that the interaction between PHSRN-GRGDSP and PEG120 is favored and the two components are well mixed at these compositions. At peptide-amphiphile molar fractions ranging from about 0.1 to 0.35, a constant value of the surface pressure is observed, pointing to a possible phase separation of the two components at these compositions.

AFM was used to characterize surface topography of the supported bioartificial membranes constructed from PEG120/PHSRN-GRGDSP mixtures and to verify miscibility of these amphiphilic molecules. Figure 4 presents typical topography and phase AFM images of mixtures at different peptide-amphiphile concentrations, acquired at room temperature in tapping mode in DI water, pH 6.5–7 as collected from the MilliQ Biocell system. Images shown are representative of the images taken over different areas on the same surface as well as of different surfaces. Images of different sizes are shown for different mixtures to provide detailed information of topography and pattern formation at various concentrations. Smaller image sizes were chosen for homogeneous surfaces to show details of their topography, whereas bigger areas were imaged on patterned surfaces to capture the presence of domains of larger size. Phase imaging provides clearer observation of fine features often not revealed by topography and can also act as a real-time contrast enhancement technique. Additionally, phase imaging can detect variations in

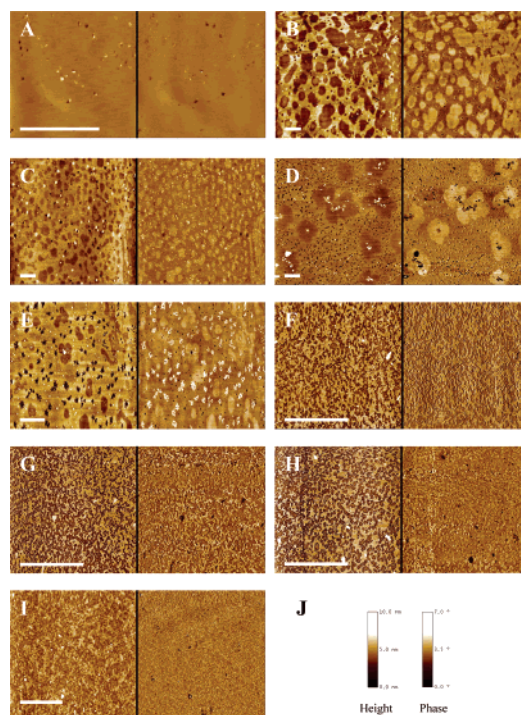


**Figure 4.** Height (left) and phase (right) images (tapping mode AFM in DI water at pH 6.5–7, as collected from the MilliQ Biocell system) of PHSRN-GRGDSP/PEG120 mixtures, deposited at room temperature and subphase pH 7. Third-order flattening was applied to all the images and a low pass filter to 50 and 75 mol % PHSRN-GRGDSP phase images to remove the noise. The bar corresponds to 5  $\mu\text{m}$ . (A) 100% PEG120,  $8 \times 8 \mu\text{m}$ ; (B) 10 mol % PHSRN-GRGDSP and 90 mol % PEG120,  $40 \times 40 \mu\text{m}$ ; (C) 15 mol % PHSRN-GRGDSP and 85 mol % PEG120,  $40 \times 40 \mu\text{m}$ ; (D) 25 mol % PHSRN-GRGDSP and 75 mol % PEG120,  $40 \times 40 \mu\text{m}$ ; (E) 35 mol % PHSRN-GRGDSP and 65 mol % PEG120,  $25 \times 25 \mu\text{m}$ ; (F) 40 mol % PHSRN-GRGDSP and 60 mol % PEG120,  $10 \times 10 \mu\text{m}$ ; (G) 50 mol % PHSRN-GRGDSP and 50 mol % PEG120,  $10 \times 10 \mu\text{m}$ ; (H) 75 mol % PHSRN-GRGDSP and 25 mol % PEG120,  $10 \times 10 \mu\text{m}$ ; (I) 100% PHSRN-GRGDSP,  $15 \times 15 \mu\text{m}$ ; (J) scale bars for height and phase images.

composition, friction, viscoelasticity, and other properties within the sample, but it cannot provide accurate information about the height of the objects. The presence of height differences of  $2.1 \pm 0.56$  nm on the image of the 100% PHSRN-GRGDSP surface (Figure 4I) suggests that some of the headgroups of peptide-amphiphiles are bent (the fully extended headgroup length of PHSRN-GRGDSP is calculated to be 7.3 nm<sup>58</sup>). Cross-sectional analysis of the images of 75 mol % (Figure 4H), 50 mol % (Figure 4G), and 40 mol % (Figure 4F) PHSRN-GRGDSP surfaces indicated that the height differences between darker and lighter domains are in the range of 1.5–5.5 nm, which is within the upper limit of the 5.7-nm height difference between the PHSRN-GRGDSP and PEG120 headgroups for fully extended headgroups (the PEG120 headgroup length used here is 1.6 nm<sup>67</sup>). The phase images of 40, 50, and 75 mol % PHSRN-GRGDSP mixtures (Figure 4F–H) are similar to the one of the pure PHSRN-GRGDSP surface (Figure 4I) in that there are no significant color variations throughout the image. Thus, taking into account the topography of the 100% PHSRN-GRGDSP (Figure 4I), mixtures at 40, 50, and 75 mol % PHSRN-GRGDSP (Figure 4F–H) are considered to be mixed compared to phase-separated ones (10, 15, 25, and 35 mol % PHSRN-GRGDSP, Figure 4B–E).

The AFM images of the surfaces with PHSRN-GRGDSP content below 40 mol % show domain formation (Figure

(74) Maget-Dana, R. *Biochim. Biophys. Acta* **1999**, *1462*, 109.

4B–E). Cross-sectional height analysis of the AFM image of the 25 mol % PHSRN-GRGDSP membrane (Figure 4D) provided a height difference of approximately  $2 \pm 0.4$  nm between the discrete darker flower shape domains and the continuous phase. Although compression of the membranes by the AFM tip and forces between the tip and sample may affect the measurements (the more fluid matrix can be compressed at a greater extent than the solid domains), the  $2 \pm 0.4$  nm height difference is within the range difference between the theoretical length of the PHSRN-GRGDSP and PEG120 fully stretched head-groups. This observation along with the phase difference between the isolated domains and the surrounding matrix (phase image in Figure 4D) suggests that the isolated flowerlike domains consist primarily of the PEG120 amphiphiles in condensed state, whereas the PHSRN-GRGDSP amphiphiles in a more fluid state constitute the continuous network. Additional features on the AFM image of 25 mol % PHSRN-GRGDSP–75 mol % PEG120 mixture can also be seen in Figure 4D. First, the continuous phase (PHSRN-GRGDSP) has smaller dark domains that appear to be PEG120 on the basis of the height difference of approximately 5 nm compared to the surrounding matrix. Second, in the middle of most of the dark flower shape domains on the height image, one can see very tall features (bright color on the height image). This is also evident on the phase image of Figure 4D as dark spots in the middle of the bright flower shape domains, which implies that there is a difference in the surface physical characteristics of the bright flower and the dark center, such as for example elasticity, and may be attributed to impurities trapped in the middle of the PEG120 crystalline domains. These impurities are also observed on the height and phase images of 100% PEG120 (Figure 4A).

The fraction of the surface area of the 10, 15, 25, and 35 mol % PHSRN-GRGDSP images occupied by darker domains decreases as PEG120 concentration is reduced (Figure 4B–E). This observation along with the height measurements and bearing analysis (which provides information on the distribution of surface levels) suggests that the darker domains on these images correspond to the condensed PEG120 phase. Thus, mixtures at 10, 15, 25, and 35 mol % of PHSRN-GRGDSP exhibit phase separation into the condensed PEG120 domains and an expanded PHSRN-GRGDSP matrix (Figure 4B–E). However, the shape of the PEG120 domains and their size vary with monolayer composition. The 90 mol % PEG120 mixture (Figure 4B) displays mostly round-shape domains of PEG120 of varying size, with some of them being interconnected. As the PEG120 concentration decreases to 85 mol % (Figure 4C), the domains become smaller and more evenly dispersed throughout the image. The 75 mol % PEG120 image (Figure 4D) reveals larger flowerlike domains of PEG120, which decrease in size as the concentration of PEG120 decreases to 65 mol % (Figure 4E). Additional smaller dark areas of irregular shape are visible on all the images but are more pronounced in Figure 4D–E.

The shape of the domains is thought to be controlled by a combination of electrostatic repulsion and interfacial line tension along the boundaries, which act in opposite directions. Electrostatic repulsion and the presence of impurities tend to favor elongated domains, whereas line tension (solid–fluid interfacial free energy) favors more circular domains.<sup>75</sup> In the initial steps of domain formation,

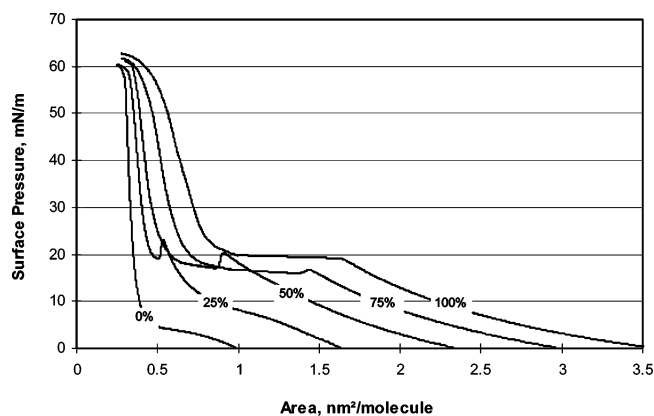


**Figure 5.** Surface pressure–area isotherms of NTFR, PEG120, and their mixtures on a DI water subphase at pH 10 and room temperature. Molar percentages of NTFR in NTFR/PEG120 mixtures are shown for each isotherm.

which in general can be understood as a diffusion-limited aggregation process, a rough domain boundary is favored.<sup>69</sup> During the growth period, the line tension tends to smooth the boundary, leading to the formation of regular shape domains such as disks, lamellae, or spirals.<sup>69</sup> However, in other cases, smoothing may not be complete over the duration of the experiment, and as a result irregular-shaped structures, such as flowers or clover leaves, are formed.<sup>69</sup> In our study, such an effect was more pronounced for the 75 mol % PEG120 mixture (Figure 4D), which exhibits larger and more isolated flowerlike domains.

To investigate the effect of the concentration and subphase pH on the miscibility of binary mixtures of peptide-amphiphiles with a different bioactive headgroup and lipidated PEG120, compression LB isotherms of NTFR peptide-amphiphiles and their mixtures with PEG120 at the air/water interface were recorded at room temperature and pH 10 (Figure 5). Here, deposition was done from water at pH 10, however, membranes were stored and imaged in MilliQ Biocell water of pH around 7. For the pure NTFR isotherm, an expanded phase was detectable at  $3.6 \text{ nm}^2/\text{molecule}$  that underwent a noticeable transition at  $1.6 \text{ nm}^2/\text{molecule}$  (LE–LC coexisting region) and was compressed into a condensed phase at surface pressures greater than 25 mN/m before it collapsed above 60 mN/m. The LE–LC coexisting region observed for the 100% NTFR isotherm persists on the isotherms of the NTFR – PEG120 mixtures, although the range of the mean molecular areas corresponding to this transition diminishes with increasing PEG120 concentration. Additionally, Figure 5 shows a “hump” on the isotherms of the peptide-amphiphile mixtures with PEG120, similar to the one observed in Figure 1, which is believed to be associated with a transition of the long peptide headgroups from a globular to an extended conformation at the air/water interface.<sup>58,68</sup> For the NTFR–PEG120 mixtures, the surface pressure gradually increased as the NTFR–PEG120 monolayers were compressed, and at surface areas of  $0.32\text{--}0.35 \text{ nm}^2/\text{molecule}$  no further compression was possible and the mixed monolayers collapsed at surface pressures of approximately 60–62 mN/m. The shape of the pure PEG120 isotherm recorded on a subphase at pH 10 is similar to the one at pH 7 (Figure 1) with a well-pronounced LE–LC coexisting region and collapse pressure at around 60 mN/m. However, the onset of the LE phase for the pure PEG120 at pH 7 was detected at a higher mean molecular area ( $1.3 \text{ nm}^2/\text{molecule}$ ) versus the one at pH 10 ( $0.9 \text{ nm}^2/\text{molecule}$ ).

(75) Keller, D. J.; McConnell, H. M.; Moy, V. T. *J. Phys. Chem.* **1986**, *90*, 29311.

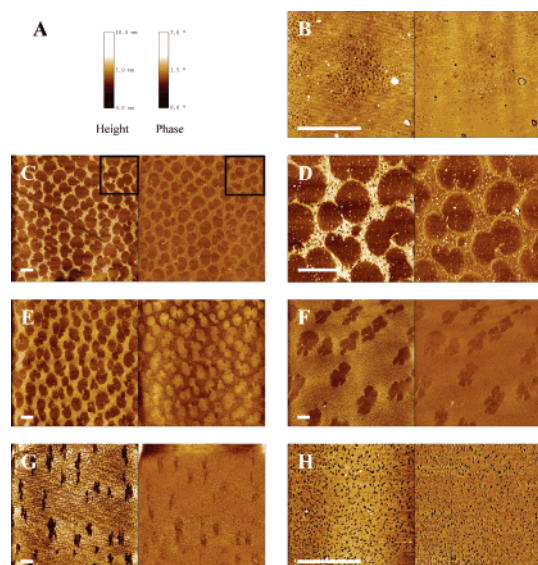


**Figure 6.** Height (left) and phase (right) images (tapping mode AFM in DI water at pH 6.5–7, as collected from the MilliQ Biocell system) of NTFR–PEG120 mixtures, deposited at room temperature and subphase pH 10. Third-order flattening was applied to all the images and a low pass filter to the 100 and 75 mol % NTFR images to remove the noise. The bar corresponds to 5  $\mu\text{m}$ . (A) Scale bars for height and phase images; (B) 100% PEG120, 10  $\times$  10  $\mu\text{m}$ ; (C) 25 mol % NTFR and 75 mol % PEG120, 50  $\times$  50  $\mu\text{m}$ ; (D) 25 mol % NTFR and 75 mol % PEG120, 15  $\times$  15  $\mu\text{m}$ , zoom-in of the areas outlined on image C; (E) 35 mol % NTFR and 65 mol % PEG120, 50  $\times$  50  $\mu\text{m}$ ; (F) 65 mol % NTFR and 35 mol % PEG120, 50  $\times$  50  $\mu\text{m}$ ; (G) 75 mol % NTFR and 25 mol % PEG120, 50  $\times$  50  $\mu\text{m}$ ; (H) 100% NTFR, 10  $\times$  10  $\mu\text{m}$ .

AFM images of the NTFR/PEG120 monolayers, deposited on hydrophobized mica from a subphase at pH 10, are presented in Figure 6. These monolayers were found to exhibit extensive lateral separation into condensed PEG120-rich domains and a liquidlike NTFR matrix at all compositions (representative concentrations of mixtures are shown in Figure 6C–G).

Bearing and cross-sectional height analysis of the NTFR/PEG120 mixtures was used to evaluate composition of the domains observed on the AFM images. Following this analysis, we assigned isolated domains to a condensed PEG120-rich phase and the surrounding matrix to a more expanded NTFR-rich phase (Figure 6) on the basis of the following evidence. First, solidlike PEG120 domains are expected to be 5.7 nm shorter than the more fluidlike NTFR matrix (the fully extended NTFR headgroup is calculated to be approximately 7.3 nm<sup>59</sup> and the PEG120 headgroup is 1.6 nm<sup>62</sup>). The height differences between the darker domains and the continuous phase for the 25, 35, 65, and 75 mol % NTFR surfaces (Figure 6C, E–G) were estimated using cross-sectional height analysis of the AFM images to be  $4.2 \pm 0.3$  nm,  $3.65 \pm 0.32$  nm,  $3.5 \pm 0.75$  nm, and  $3.9 \pm 0.68$  nm, respectively, which is within the maximum 5.7 nm theoretical height difference between the NTFR and PEG120. Additionally, the dark pinhole domains, dispersed within the lighter NTFR matrix, for example, on the 75% PEG120 mixture (Figure 6D), are of the same 4.5 nm depth as the larger, dark round-shaped domains (Figure 6D), which is within the 5.7 nm theoretical difference between NTFR and PEG120 fully stretched headgroups. This observation suggests that some of the PEG120 molecules are dispersed throughout the liquid-expanded (LE) NTFR matrix. Second, bearing analysis of the height images provided evidence that the fraction of all the shorter (dark color) areas increased

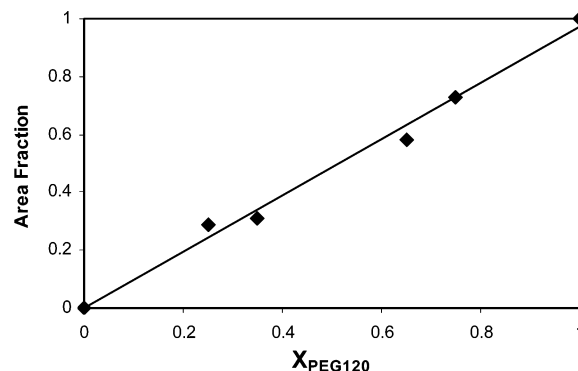


**Figure 7.** Area fraction of the shorter domains on the NTFR–PEG120 LB films, measured using bearing analysis of the AFM height images in Figure 6 versus the molar fraction of PEG120 in the mixture ( $X_{\text{PEG120}}$ ). The line represents the linear fit to the data with slope = 0.973 and correlation coefficient  $R^2 = 0.99$ .

linearly with increasing PEG120 mol fraction (for  $x_{\text{PEG120}} = 0.25$ – $0.75$ ), as would be expected if the shorter, dark color areas were PEG120 (Figure 7). Additional features observed on the 100% NTFR monolayer are small dark areas of an average depth of  $8.8 \pm 1$  nm (Figure 6H), suggesting that there could be missing peptide-amphiphile molecules within the monolayer (total theoretical length of the fully stretched NTFR peptide-amphiphile was calculated to be approximately 8.9 nm<sup>59</sup>).

The shape of the PEG120 domains changes as the PEG120 concentration decreases from mostly round (spherical or bean-shaped) for the 75% and 65% PEG120 (Figure 6C–E) to flowerlike for the 35% PEG120 (Figure 6F) and elongated flowers for the 25% PEG120 image (Figure 6G). The round-shaped domains observed on the 75% PEG120 (Figure 6C and D) image seem to aggregate into clusters on the image of the 65% PEG120 monolayer (Figure 6E) and into flowerlike domains for the 35% PEG120 (Figure 6F).

Interestingly, as can be seen in Figure 4B–E and in Figure 6C–G, when the PEG120 concentration decreases (to a different extent for these two systems), the shape of the condensed PEG120 domains changes from mostly round to flowerlike of varying size. Flowers usually form when the boundaries of the domains are not smoothed by the line tension (i.e., interfacial free energy between solid domains and fluid matrix) during the experiment, which suggests that most probably more time is required for the line tension to give a smoother boundary when there is less PEG120 present in the monolayer.

To investigate the effect of subphase pH on miscibility and pattern formation in peptide-amphiphile/phospholipid mixtures, NTFR peptide-amphiphiles were mixed with a short phospholipid DPPC at 50 and 75 mol % NTFR. AFM images of these surfaces were recorded and analyzed similarly to the NTFR–PEG120 mixtures. Figure 8 presents topography and phase AFM images of NTFR–DPPC mixtures deposited from water subphase at pH 7 and 10. All images were taken at room temperature in tapping mode in DI water at pH 6.5–7 (as collected from the MilliQ Biocell system). Absence of any pronounced features on the phase images of the 50% NTFR–50% DPPC (Figure 8A) and 75% NTFR–25% DPPC (Figure 8B) surfaces deposited at pH 7 suggests that the NTFR and DPPC formed mixed interfaces at these concentrations. For comparison, AFM images of the 50% NTFR–50% DPPC and 75% NTFR–25% DPPC surfaces deposited at pH 10 are shown in Figure 8C–D, respectively. Extensive lateral phase separation is observed for both the NTFR/DPPC mixtures tested, similar to NTFR/

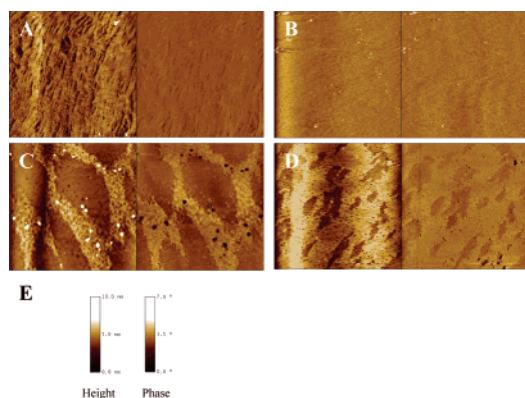


**Figure 8.** Comparison of NTFR-DPPC membranes deposited at neutral and alkaline pH. Height (left) and phase (right) images (tapping mode AFM in DI water at pH 6.5–7, as collected from the MilliQ Biocell system) of NTFR-DPPC mixtures, deposited at room temperature from DI water subphase at indicated pH. All images are  $15 \times 15 \mu\text{m}$ . Third-order flattening and a low pass filter was applied to all the images. (A) 50 mol % NTFR and 50 mol % DPPC deposited at pH 7. (B) 75 mol % NTFR and 25 mol % DPPC deposited at pH 7. (C) 50 mol % NTFR and 50 mol % DPPC deposited at pH 10. (D) 75 mol % NTFR and 25 mol % DPPC deposited at pH 10. (E) Scale bars for height and phase images.

PEG120 mixtures (Figure 6). Cross-sectional analysis of the height images of 75% NTFR–25% DPPC (Figure 8D) and 50% NTFR–50% DPPC (Figure 8C) surfaces indicated that the height differences between the shorter (DPPC) domains, shown with a dark color, and the taller (NTFR) domains, shown with a light color, are  $3.06 \pm 0.50 \text{ nm}$ , which is within the upper limit of the 6.2-nm height difference between the NTFR and DPPC for fully extended headgroups. The NTFR headgroup was calculated to be approximately 7.3 nm and the DPPC headgroup length was  $1.15 \pm 0.15 \text{ nm}$  for solid-phase monolayers.<sup>76</sup>

The NTFR peptide has a negative charge at both pH 7 and pH 10. PEG120, on the other hand, is a nonionic surfactant which has been shown to acquire a negative charge at both pH 7 and 10 via preferential adsorption of hydroxyl ions.<sup>77,78</sup> When mixed with NTFR at pH 10, PEG120 separates into solidlike domains within the continuous matrix of NTFR at all concentrations (Figure 6). Likewise, when NTFR is mixed with DPPC at pH 10, which is neutral at this pH,<sup>79</sup> phase separation occurs for both of the compositions tested (50 and 75 mol % NTFR, Figure 8C–D). However, when NTFR/DPPC mixtures are deposited from subphase at pH 7, well-mixed interfaces are formed (Figure 8A–B). Additionally, when PHSRN-GRGDSP, which has an overall positive charge at pH 7, is mixed with lipidated PEG120 (with acquired negative

charge at pH 7 in water) on the subphase at pH 7, phase separation occurs in a concentration-dependent manner (Figure 4). In all cases, however, when phase separation occurs and patterns are formed, independent of whether the peptide headgroup has a positive or a negative charge, the PEG120 and DPPC form isolated solidlike domains within a peptide-amphiphile fluidlike continuous matrix.

Thus, mixing behavior of peptide-amphiphile/phospholipid mixtures and pattern formation can be controlled by varying peptide-amphiphile concentration or subphase pH. These parameters can be easily adjusted and thus offer a convenient way for creating biomimetic patterned membranes. Additionally, the shape and size of the patterns seem to be influenced by line tension, diffusion, and the time that these mixtures are let to equilibrate before deposition. However, the effect of these parameters was not investigated in detail in this study. Instead, time intervals between spreading and compression as well as time between compression and deposition were kept the same for all the mixtures.

## Conclusions

The focus of this study was to investigate the mixing behavior in binary mixtures of peptide-amphiphiles and lipidated PEG120 or phospholipids as well as to study the morphology and pattern formation in supported LB membranes. Thermodynamic analysis of surface pressure–area LB isotherms for peptide-amphiphile/PEG120 mixtures on DI water subphase was performed to evaluate the extent of miscibility of the two molecules. AFM was used to obtain high-resolution images of supported LB membranes and thus to characterize their surface topography and pattern formation. The effect of monolayer composition and subphase pH on surface morphology was investigated.

Our results demonstrated that patterned interfaces can be created and manipulated using peptide-amphiphiles along with commonly studied phospholipids in a concentration- or pH-dependent manner. Analysis of the AFM images of the phase-separated membranes indicated that the isolated domains consisted mainly of condensed lipidated PEG120 or DPPC, whereas the continuous matrix was attributed to a more fluidlike peptide-amphiphile (PHSRN-GRGDSP or NTFR). The PHSRN-GRGDSP peptide-amphiphile exhibited a concentration-dependent phase separation at pH 7. Additionally, for the NTFR peptide-amphiphile, the subphase pH at deposition had a pronounced effect on the miscibility, thus providing another way to control (or induce) phase separation in phospholipid/peptide-amphiphile mixtures. These two parameters, concentration and pH, are easy to control and thus can be employed in creating bioactive surfaces with desired patterns of differing functionalities.

**Acknowledgment.** The NTFR LB isotherms and the raw AFM images of NTFR were collected by R.W. Kasinskas. Acknowledgment is made to the Donors of the American Chemical Society Petroleum Research Fund for partial support of this research under 39120-G4.

LA0468085

(76) Brumm, T.; Naumann, C.; Sackmann, E.; Rennie, Ar.; Thomas, R. K.; Kanellas, D.; Penfold, J.; Bayerl, T. M. *Eur. Biophys. J.* **1994**, *23*, 289.

(77) Chan, Y.-H. M.; Schweiss, R.; Werner, C.; Grunze, M. *Langmuir* **2003**, *19*, 7380.

(78) Kreuzer, H. J.; Wang, R. L. C.; Grunze, M. *J. Am. Chem. Soc.* **2003**, *125*, 8384.

(79) Liu, h.; Lu, R. Z.; Turcotte, J. G.; Notter, R. H. *J. Colloid Interface Sci.* **1994**, *167*, 378.